


## Article

# Structural Optimization of Annular Thermoelectric Module Applied to Liquefied Natural Gas Cold Energy Recovery

Yulong Zhao <sup>1</sup>, Hongmei Diao <sup>1</sup>, Wenjie Li <sup>1</sup>, Zhiwei Xuan <sup>1</sup>, Qi Zhang <sup>1</sup>, Yulin Wang <sup>2,\*</sup>  and Minghui Ge <sup>1,\*</sup>

<sup>1</sup> Hebei Key Laboratory of Thermal Science and Energy Clean Utilization, Hebei University of Technology, Tianjin 300401, China

<sup>2</sup> Tianjin Key Laboratory of Refrigeration Technology, Tianjin University of Commerce, Tianjin 300134, China

\* Correspondence: wangylfcs@gmail.com (Y.W.); geminghui@hebut.edu.cn (M.G.)

**Abstract:** The gasification of liquefied natural gas (LNG) is characterized by a substantial release of cold energy, which can be utilized for power generation via thermoelectric generator (TEG). Employing a gasifier integrated with a thermoelectric generator for LNG gasification allows for the recovery of cold energy and its conversion to useful power, a process that holds significant potential for widespread application. In the study, a thermoelectric model has been developed for an annular thermoelectric module, which formed a new category of gasifier tube. The influence of the module's structure as well as the heat transfer parameters on the thermoelectric performance was examined. The results revealed that an optimum height of the thermoelectric leg, specifically 2 mm, maximized the output power while allowing the thermoelectric conversion efficiency to reach a peak of 3.25%. Another noteworthy finding is that an increase in the central angle of the thermoelectric leg leads to a concomitant rise in output power but a decrease in conversion efficiency. Furthermore, when the heat transfer coefficients at the hot and cold ends of the module achieved 4000 W/(m<sup>2</sup>·K) and 10,000 W/(m<sup>2</sup>·K), respectively, the conversion efficiency can be elevated to 6.98%. However, any additional enhancement in power generation performance derived from further augmenting the heat transfer is marginal. These findings can serve as a valuable reference in the design and optimization of TEG intended for the recovery of cold energy from LNG.

**Keywords:** liquefied natural gas; cold energy; thermoelectric; annular; structural optimization



**Citation:** Zhao, Y.; Diao, H.; Li, W.; Xuan, Z.; Zhang, Q.; Wang, Y.; Ge, M. Structural Optimization of Annular Thermoelectric Module Applied to Liquefied Natural Gas Cold Energy Recovery. *Processes* **2023**, *11*, 2687. <https://doi.org/10.3390/pr11092687>

Academic Editor: Kun Wang

Received: 16 August 2023

Revised: 29 August 2023

Accepted: 5 September 2023

Published: 7 September 2023



**Copyright:** © 2023 by the authors. Licensee MDPI, Basel, Switzerland. This article is an open access article distributed under the terms and conditions of the Creative Commons Attribution (CC BY) license (<https://creativecommons.org/licenses/by/4.0/>).

## 1. Introduction

The demand for energy has been steadily increasing as a result of economic growth and improvements in people's living standards. Global energy consumption and trade statistics indicate an annual growth rate of 2.6% [1]. Natural gas, being a cleaner alternative to coal and oil, has witnessed a rising share in energy consumption. To facilitate the long-distance transportation of natural gas, it is liquefied at low temperatures to form liquefied natural gas (LNG). At LNG receiving terminals, the LNG, which is maintained at −162 °C, needs to undergo a heating and gasification process before it can be delivered to customer terminals. Throughout the gasification process, each ton of LNG releases approximately 840 MJ [2,3] of cold energy, and the recovery of this LNG cold energy offers substantial economic and environmental benefits.

Presently, there exist several methods for the utilization of LNG cold energy, including air separation [4], refrigerated storage [5,6], CO<sub>2</sub> capture [7], seawater desalination [8], and power generation [9]. Among these, power generation is considered to be one of the most efficient approaches for harnessing LNG cold energy. Power generation from LNG cold energy can be achieved through two primary means: power cycles and thermoelectric generators. Power cycles encompass various techniques such as direct expansion [10], organic Rankine cycle [11], and combined cycle [12]. Power cycles offer a wide range of applications, characterized by their high thermal efficiency and substantial power generation capacity. Bao et al. [13] implemented a two-stage condensing Rankine cycle system to

effectively enhance the efficiency of an LNG cold energy generation system, achieving a thermal efficiency of up to 10.07%. Joy et al. [14] observed that LNG vaporization under higher pressures yielded greater power output. Ma et al. [15] established a multi-stage Rankine cycle for LNG cold energy recovery and discovered that the growth of power generation decelerated with an increase in the number of stages within the multi-stage Rankine cycle. Zhou et al. [16] developed an innovative LNG cold energy utilization system that integrated an organic Rankine cycle, a transcritical carbon dioxide cycle, carbon dioxide storage, a seawater ice cycle, and a combustion power generation system. Their findings indicated that the net power generation of the ORC surpassed that of other working fluids when R290 and R1270 were employed as the working fluids. Choi et al. [17] proposed a novel approach for recovering LNG cold energy through power generation using a cascaded Rankine cycle. They achieved a thermal efficiency of up to 12.5% in a three-stage tandem Rankine cycle utilizing propane as the working fluid. Qu et al. [18] introduced a vaporizer system for recovering LNG cold energy through an organic Rankine cycle. Their investigation revealed that an increase in the LNG inlet temperature led to a reduction in the system's power output, while the thermal efficiency of the system improved. Yu et al. [19] developed an LNG cold energy power generation system utilizing seawater as a heat source and observed a rapid decline in the net output power of the system with increasing LNG target pressure, noting that the system achieved the largest net output power when R1270 was employed. However, these systems entail complex equipment, substantial costs, extensive spatial requirements, and necessitate a reliable and abundant source of cold energy during operation. Consequently, their predominant utilization is observed in large-scale LNG gasification stations. In the huge number of LNG satellite stations, where the LNG gasification volume is small and the flow rate fluctuates greatly, the utilization rate of cold energy remains notably low. Employing a thermoelectric generator for the recovery of LNG cold energy emerges as a more favorable choice.

Thermoelectric generators are widely used in waste heat recovery as they are devoid of moving part edges, noise, and wear and tear, have a small volume and a long service life, and are lightweight and easy to move [20,21]. LNG cold energy thermoelectric generator refers to the usage of LNG as the cold source and seawater or air as the heat source, thereby constructing a temperature difference between the hot and cold ends (TDHC) of the thermoelectric module (TEM) and achieving the recovery of cold energy to generate electricity. Although the efficiency of utilizing thermoelectric generators to recover LNG cold energy for power generation is lower compared with power cycles, their high reliability and broader applicability make them more promising for implementation in LNG satellite stations. Kambe et al. [22] constructed a thermoelectric generator using water as the heat source and liquid nitrogen as the cold source, and the thermoelectric conversion efficiency of the BiTe-based TEM could reach 3.5% at 0 °C at the hot end and −120 °C at the cold end. Weng et al. [23] attached four TEMs to the outlet of a liquid nitrogen tank and obtained 0.93 W of output power at a liquid nitrogen flow rate of 3.6 g/s. Lin et al. [24] proposed a conversion efficiency of 2.67% by utilizing the two ends of the TEM constituted by the warmed-up nitrogen and liquid nitrogen. Lobunets et al. [25] integrated a seawater gasifier with TEM to develop an LNG cold energy thermoelectric generator. The generator utilized liquid nitrogen as the cold source and 62 °C hot water as the hot source. The maximum power generation efficiency was reported to be 8.85%.

The low-temperature characteristics of the TEM directly determine the theoretical conversion efficiency of LNG cold energy, and the thermoelectric features of the TEM under a low-temperature environment are critical. Chung et al. [26] developed high-performance thermoelectric materials for application in the low-temperature region, which were able to reach a high value of ZT of 0.8 up to 225 K. Sun et al. [27] modeled the analytical solution of TEM and the maximum efficiency of the TEM can be up to 9% under the conditions of 130 K and 290 K for the temperatures of cold and hot sides, respectively. Kambe et al. [28] found that when a conventional BiTe-based TEM was used to recover liquid nitrogen cold energy of liquid nitrogen for power generation, the TEM was prone to deformation, causing

a sudden drop in output power when the temperature at the cold end was reduced to  $-160\text{ }^{\circ}\text{C}$ . The module is also found to have a higher output power than the conventional BiTe-based TEM. Karabetoglu et al. [29] built a test system for thermoelectric generators and tested the Seebeck coefficient as well as the resistance of TEM in the range of 100–375 K. Jeong [30] developed an analytical model of a TEM and analyzed the impacts of contact resistance, contact thermal resistance, as well as cold-end heat transfer on the thermoelectric performance and the optimal height of thermoelectric leg (TEL) at low temperatures.

In summary, preliminary investigations have been carried out on the viability of employing thermoelectric generators for the recovery of LNG cold energy, affirming the feasibility of this technology. The authors [31] have designed a new gasifier tube with a thermoelectric generator to generate power with a density of about  $20.8\text{ W/m}$  using air as the heat source. Nevertheless, the TEMs utilized in the present study are of a fixed size, and the investigation pertaining to the influence of TEM structure on system performance is absent. Consequently, the optimization of the TEM structure is anticipated to enhance the performance of LNG cold power generation further. In this study, the thermoelectric model of an annular TEM from the gasifier tube with a thermoelectric generator applied to LNG cold energy recovery is constructed. The influence of the structure of TEM on the thermoelectric performance is investigated at low temperature, and the results of the study can provide guidance for the design and performance optimization of the novel thermoelectric generator.

## 2. Mathematical Model

### 2.1. Annular Thermoelectric Module

The fundamental component of a LNG gasifier is the gasifier tube, through which LNG is introduced from the bottom. The LNG undergoes gasification by utilizing heat from the surrounding seawater or air, which heats up the LNG within the tube. The authors [31] proposed an innovative gasifier tube integrated with a thermoelectric generator, as depicted in Figure 1a. This design combines a conventional gasifier tube with annular thermoelectric generators positioned on the outer side of the tube. Consequently, the system enables the recovery of cold energy for power generation during the LNG gasification process. The newly developed gasifier with a thermoelectric generator operates without any moving parts or working medium. It can generate power as long as there is a temperature difference, without impeding the regular functioning of the LNG gasification process. Moreover, it is not constrained by fluctuations in the gasification volume, offering favorable economic prospects and broader applicability.

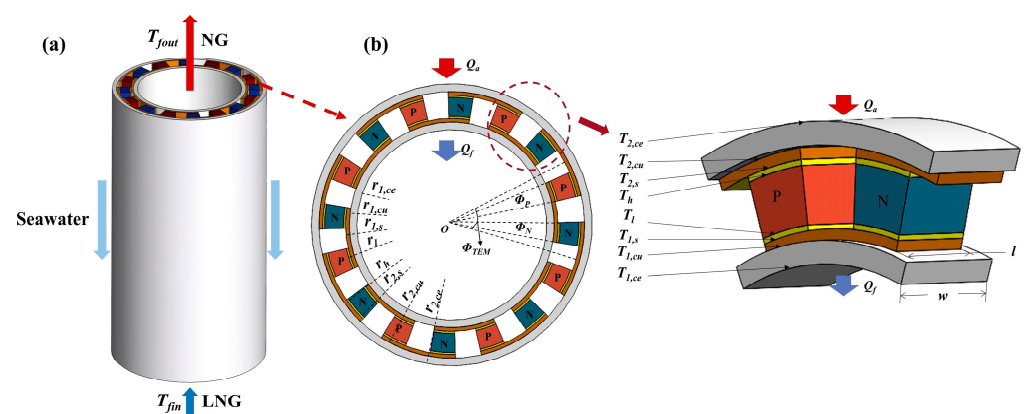


**Figure 1.** Structure diagram of important components. (a) Gasifier tube with thermoelectric generator. (b) Annular TEM structure.

The annular TEM serves as the fundamental unit within the newly developed gasifier tube, and its thermoelectric performance directly influences the efficiency of cold energy recovery. In view of this, the annular TEM is selected as the focus of the research, and a

physical model is constructed, as depicted in Figure 1b. The annular TEM primarily consists of a ceramic layer, a conductive copper sheet layer, and an annular TEL. The TEL is connected to the conductive copper sheet through soldering. Within the inner layer of the new gasifier tube, the ceramic layer has a radius of  $r_1$  and a height of  $L_{ce}$ . The conductive copper sheet has a height of  $L_{cu}$ , while the TEL has a height of  $L$ , and the solder layer has a height of  $L_s$ . The overall TEM occupies a central angle of  $\phi_{TEM}$ , with the central angle  $\phi_{P-N}$  specifically dedicated to the P-type thermoelectric leg and the N-type thermoelectric leg. The total length of the TEM is represented by  $w$ , whereas the length of the TEL is denoted as  $l$ .

In order to simplify the model, several assumptions are made as follows:

1. All surfaces, except for the hot and cold surfaces, are assumed to be insulated.
2. Contact resistance and contact thermal resistance are neglected.
3. The system is assumed to be in a steady state.

### 2.2. Thermoelectric Model

In this article, the thermoelectric coupling problem is computed, and data are processed using COMSOL Multiphysics software. The thermoelectric model takes into account the Seebeck effect, the Peltier effect, the Joule effect, and the Thomson effect [32]. The heat flux and electric charge continuity equations in the steady state of the model are expressed as follows:

$$\nabla \vec{q} = \frac{\vec{J}^2}{\lambda} \quad (1)$$

$$\nabla \vec{J} = 0 \quad (2)$$

In this case,  $\vec{q}$  stands for heat flux vector,  $\vec{J}$  stands for current density vector. The thermoelectric coupling equation will be denoted as:

$$\vec{q} = \beta \vec{J} - \kappa \nabla T \quad (3)$$

$$\vec{J} = \lambda \alpha \nabla T - \lambda \nabla U \quad (4)$$

where  $\alpha$ ,  $\beta$ ,  $T$ ,  $U$ ,  $k$ , and  $\lambda$  stand for the Seebeck coefficient, Peltier coefficient, temperature, electrical potential, thermal conductivity, and electrical conductivity, respectively.

The above equation can be rewritten as:

$$\nabla(\kappa \nabla T) + \frac{\vec{J}^2}{\lambda} - \nabla(\beta \vec{J}) = 0 \quad (5)$$

$$\nabla(\lambda \alpha \nabla T - \lambda \nabla U) = 0 \quad (6)$$

With the above equations, the temperature field as well as the potential distribution within the model can be obtained.

### 2.3. Key Parameters

The power generation performance of TEM is commonly evaluated based on key performance indicators, namely output power and conversion efficiency. In accordance with the principle of the Seebeck effect, when there exists a TDHC, an electric potential is generated in the conductor circuit, expressed as:

$$U = \alpha(T_h - T_l) = \alpha \Delta T \quad (7)$$

where  $T_h$  and  $T_l$  are the temperatures of the hot and cold sides of the TEM, respectively.

As a consequence of the inherent internal resistance of the TEM, the thermoelectric potential resulting from the conversion of absorbed thermal energy is distributed across

both the internal resistance  $R$  and the external load resistance  $R_L$ . Consequently, the actual output power  $P$  of the TEM can be expressed as follows:

$$P = UI = \frac{(\alpha\Delta T)^2 R_L}{(R + R_L)^2} \quad (8)$$

When the TEM internal resistance is equal to the load resistance, the output power of the TEM will be the maximum, i.e., the maximum output power  $P_{\max}$  is expressed as:

$$P_{\max} = \frac{(\alpha\Delta T)^2}{4R_L} \quad (9)$$

At this time, the conversion efficiency  $\eta_{\max}$  of the TEM is:

$$\eta_{\max} = \frac{P}{Q_h} \quad (10)$$

#### 2.4. Boundary Conditions

In the simulations conducted in this study, the temperature of LNG is set at 111.15 K. When the LNG undergoes flow boiling, the corresponding HTC is approximately 2200 W/(m<sup>2</sup>·K) [33]. It is important to note that the heat transfer parameters outside the tube of the LNG gasifier can vary significantly depending on the chosen gasification methods. Seawater is utilized as the heat source, the temperature is set at 273.15 K, and the HTC can reach up to 5800 W/(m<sup>2</sup>·K) [34]. The structural parameters of the TEM employed in the simulations of this study are detailed in Table 1.

**Table 1.** TEM structural parameters and operating parameters [35].

Parameter Names	Unit	Numerical Value
Structural parameters		
$\Phi_{\text{TEM}}$	°	45
$\Phi_{\text{P-N}}$	°	11.25
Cold end radius of TEM $r_{1,ce}$	mm	10
Inner ceramic plate radius $r_{1,cu}$	mm	10.8
Inner copper sheet radius $r_{1,s}$	mm	11.2
Inner welding layer radius $r_1$	mm	11.4
Height of TEL $L$	mm	5
Radius of outer welding layer $r_h$	mm	16.6
Radius of outer copper sheet $r_{2,s}$	mm	17
Radius of inner ceramic plate $r_{2,cu}$	mm	17.8
Operational parameters		
Fluid temperature inside the tube $T_f$	K	111.15
Fluid temperature outside the tube $T_a$	K	273.15
HTC outside the tube $h_a$	W/(m <sup>2</sup> ·K)	5800
HTC inside the tube $h_f$	W/(m <sup>2</sup> ·K)	2200

The TEM employs CsBi<sub>4</sub>Te<sub>6</sub> [26] as the P-type thermoelectric material and BiSb [35] as the N-type thermoelectric material, as indicated in Figure 2. These selected materials demonstrate improved thermoelectric performance within lower temperature ranges. The physical parameters of the other materials are provided in Table 2.

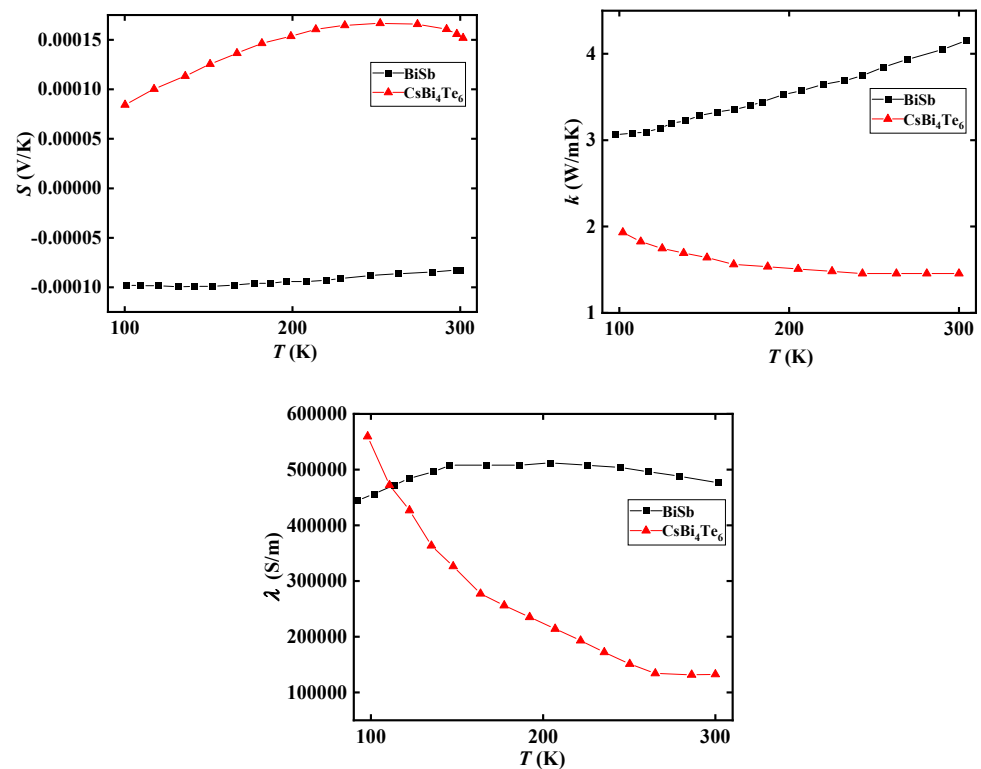


Figure 2. Thermoelectric parameters of  $\text{CsBi}_4\text{Te}_6$  and BiSb.

Table 2. Low-temperature physical parameters of TEM [36–39].

Materials	Density (kg/m <sup>3</sup> )	Specific Heat Capacity (J/kg·K)	Heat Conductivity (W/m·K)	Conductivity (S/m)
BiSb	7858	154		
$\text{CsBi}_4\text{Te}_6$	6858	154		
Copper	8940	385	385	$5.88 \times 10^7$
Ceramics	3900	880	25	
Welding layer	7260	230	55	$2 \times 10^7$

### 2.5. Grid-Independent Verification

The mathematical model is discretized using a tetrahedral mesh, as illustrated in Figure 3. To ensure the accuracy and reliability of the computational results, grid-independent verification of the mathematical model is performed. Table 3 presents a comparison of the output power and heat transfer capacity of the TEM at a TEL height of 8 mm for varying numbers of grids. It is observed that after reaching a grid number of 19,313, further increments do not significantly affect the results. Consequently, for the purposes of this study, a grid number of 19,313 is chosen.

Table 3. Grid-independent verification of TEM.

Number of Grids	$Q_h$ (Inaccuracy)	$P$ (Inaccuracy)
8035	0.58591 W (0.012%)	0.029104 W (0.02%)
12,469	0.58588 W (0.007%)	0.029101 W (0.01%)
19,313	0.58584 W	0.029098 W
35,992	0.58584 W	0.029098 W

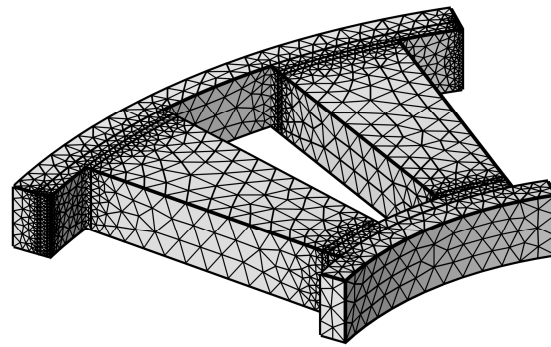


**Figure 3.** Finite element model of TEM.

### 2.6. Model Verification

In order to validate the reliability of the proposed model, this study conducts a comparative analysis between the simulation results obtained and those reported in the literature [38], as depicted in Figure 4. The TEM structure examined in the literature [38] features a flat plate configuration with  $\text{Bi}_2\text{Te}_3$  as thermoelectric material. The hot and cold side temperatures of the TEM are set to 300 K and 400 K, respectively. Under steady-state conditions, the influence of the TEM's thermoelectric properties is investigated for a central angle of  $11.25^\circ$  and TEL heights ranging from 1 mm to 9 mm. The results obtained from the model calculations in this study exhibit a high level of agreement with the findings reported in the literature, with an error margin within 2%. This close correspondence between the simulation results and literature data provides strong evidence supporting the reliability of the proposed model.

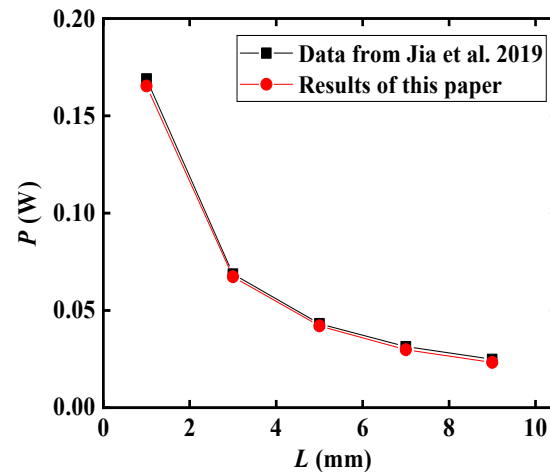


**Figure 4.** Verification of simulation results [38].

## 3. Results and Discussion

### 3.1. Effect of TEL Height

In this research, we initially investigate the variation in thermoelectric performance of the TEM with respect to load resistance at different heights of the TEL. The results are presented in Figure 5. It is worth noting that as the load resistance increases, the output power and conversion efficiency of the TEM exhibit an initial increase followed by a decrease. This indicates the presence of an optimal load resistance that yields the highest thermoelectric performance for the TEM. This behavior is closely associated with the internal resistance of the TEM. When the internal resistance of the TEM matches the external load resistance, the TEM achieves maximum output power. Furthermore, the figure illustrates that the optimal load resistance varies with different TEL heights. As the TEL height increases, the internal resistance of the TEM also increases, leading to an

increase in the optimal load resistance. In the subsequent analysis of influencing factors, the optimal load resistance is considered as the external resistance.

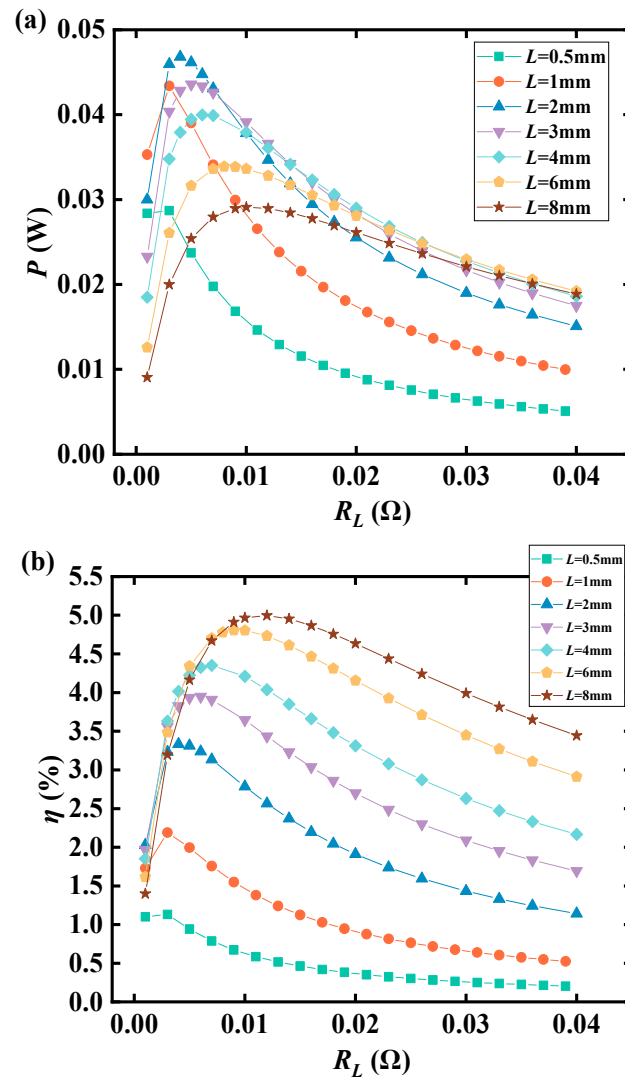


**Figure 5.** Variation of thermoelectric performance of TEM with load resistance for different TEL heights. (a) Output power. (b) Conversion efficiency.

Figure 5 reveals an additional observation that the maximum output power initially increases and then decreases as the TEL height increases. At a TEL height of 2 mm, the output power reaches its peak value of 0.047 W, while the conversion efficiency continues to rise with increasing TEL height. To further analyze these variations, Figure 6 presents the influence of TEL height on key parameters of the TEM. As the TEL height increases, the thermal resistance of the TEM gradually rises, resulting in reduced heat transfer through the TEM under identical hot and cold side heat transfer conditions. Simultaneously, the TDHC increases due to the greater proportion of the TEMs thermal resistance in the overall heat transfer thermal resistance. A higher TDHC value corresponds to a higher thermoelectric conversion efficiency for the TEM. Therefore, as the TEL height increases, the module conversion efficiency gradually improves. The output power of the TEM is essentially the product of the heat transfer quantity and the conversion efficiency. Consequently, the existence of an optimal TEL height maximizes the output power through the combined effect of these two factors.



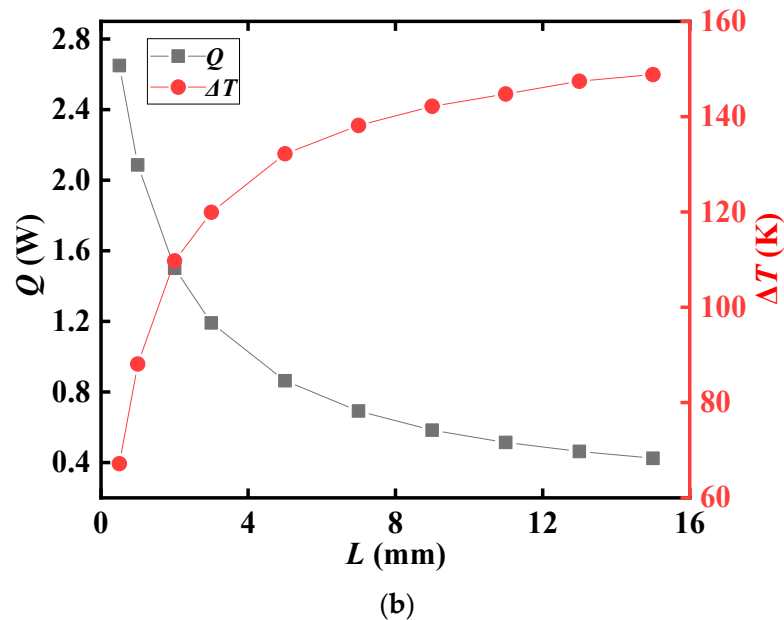
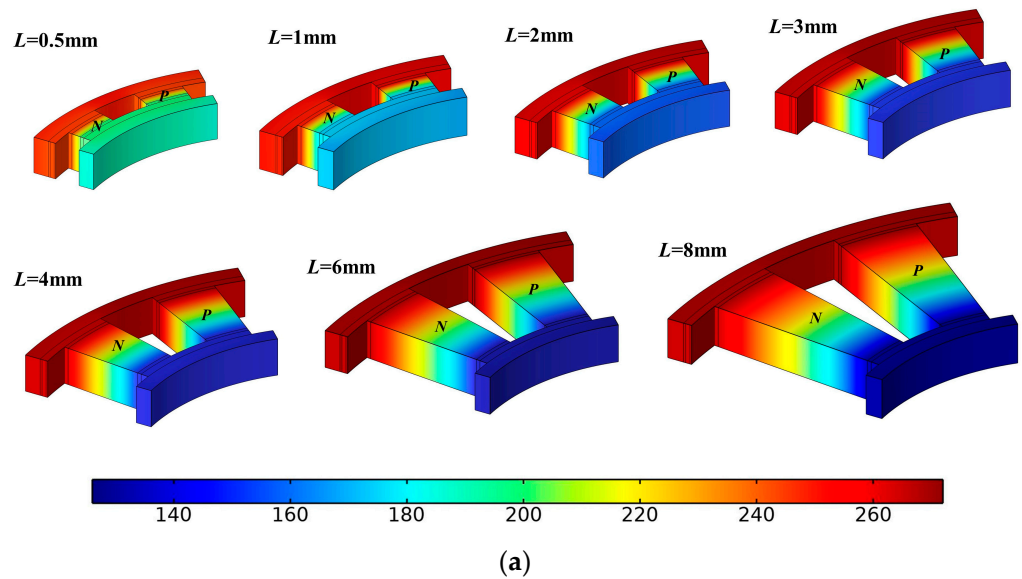


**Figure 6.** Effect of TEL height on module key parameters. (a) Temperature cloud diagram. (b) Heat exchange capacity and TDHC.

### 3.2. Effect of TEL Central Angle

The influence of the central angle of the TEL on the thermoelectric performance of the TEM is further investigated, as illustrated in Figure 7. With an increase in the central angle of the TEL, the output power gradually rises while the efficiency gradually declines. Specifically, at a TEL height of 2 mm, when the TEL central angle increases from  $8.5^\circ$  to  $14.5^\circ$ , the output power of the TEM experiences a 10.9% increase, whereas the conversion efficiency decreases by 22.34%. Furthermore, the figure indicates that the impact of the central angle variation diminishes as the TEL height increases.

The variation in the heat exchange capacity of the TEM with respect to the central angle of the TEL is depicted in Figure 8. It can be observed that the heat exchange capacity increases gradually as the TEL central angle increases. An increase in the TEL central angle leads to a reduction in the thermal resistance of the TEM. Consequently, the heat exchange capacity of the TEM increases.

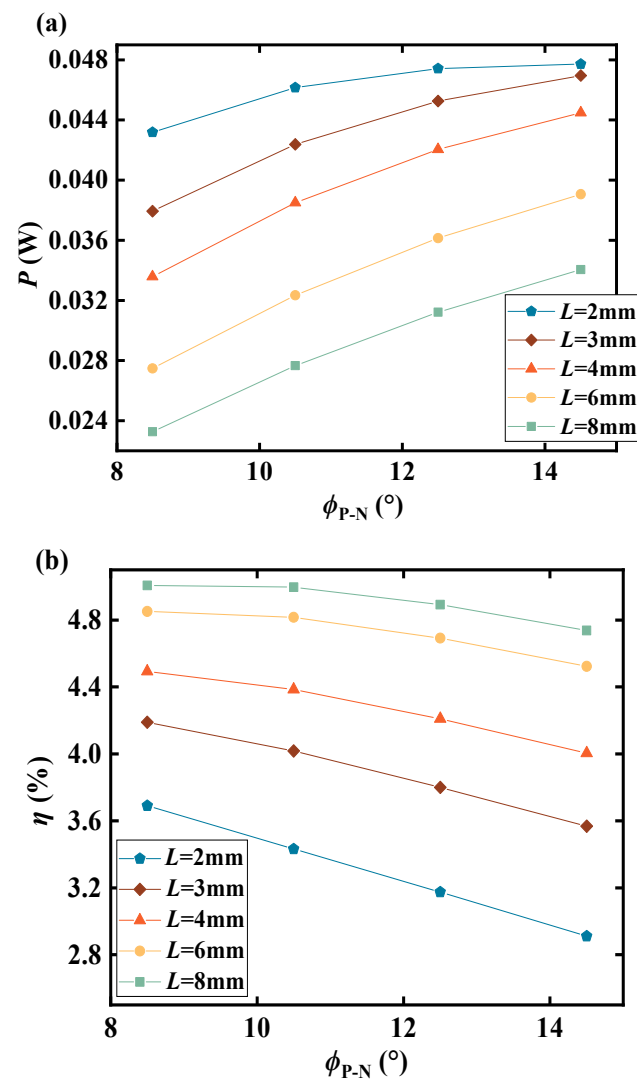


Figure 7. Variation of thermoelectric performance of TEM with central angle of TEL. (a) Output power. (b) Conversion efficiency.

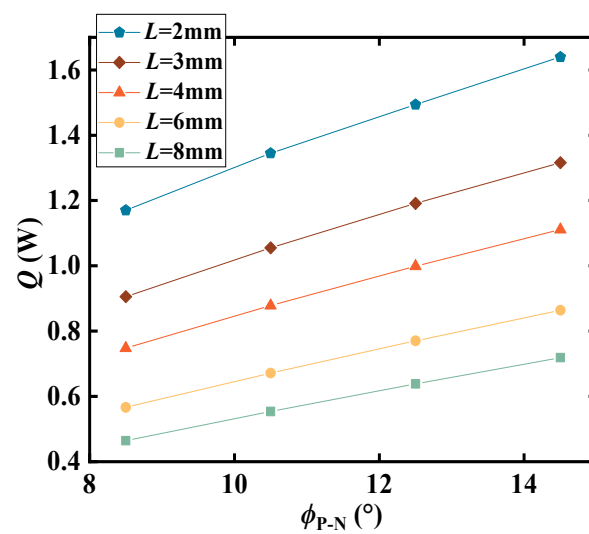
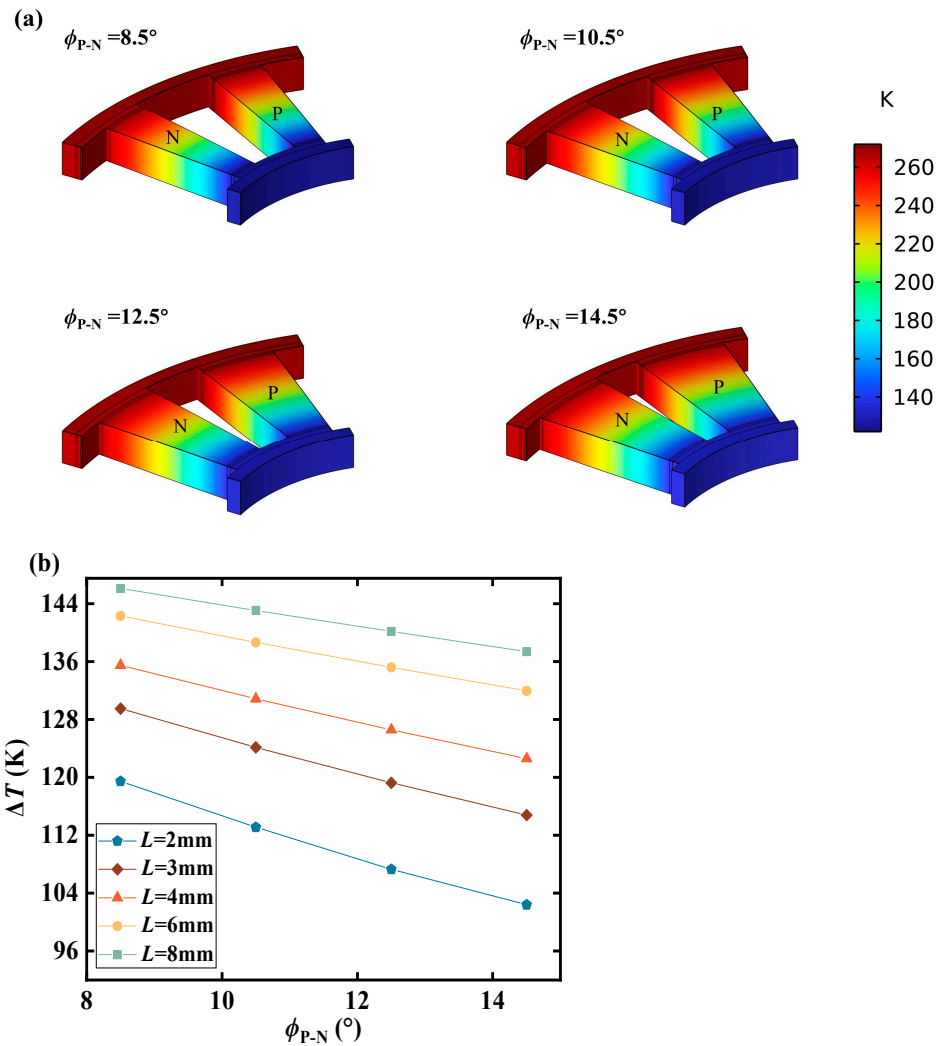


Figure 8. Variation of heat exchanger capacity of TEM with central angle of TEL.

The temperature distribution within the TEM is influenced by the central angle of the TEL, as illustrated in Figure 9. However, it is observed that the variation in the central angle has minimal impact on the temperature distribution of the TEM. On the other hand, the TDHC decreases with an increase in the TEL central angle, which consequently leads to a decrease in conversion efficiency. Furthermore, it is noteworthy that when the TEL height is large, the change in the central angle of the TEL results in a relatively small variation in thermal resistance. Consequently, the heat exchange capacity and TDHC undergo less significant changes, thereby reducing the impact of central angle variation on the thermoelectric performance of the TEM.



**Figure 9.** Variation of temperature parameters with central angle of TEL. (a) Temperature cloud diagram ( $L = 5$  mm). (b) Temperature difference between hot and cold ends.

### 3.3. Influence of Heat Exchange

The alteration of heat transfer parameters in the cold and hot sources results in changes to the HTCs inside and outside the tube, thereby inevitably impacting the performance of the generator. The influence of HTCs inside and outside the tube on the thermoelectric performance of the TEM is depicted in Figure 10. The figure illustrates that the output power and efficiency increase with higher HTCs inside and outside the tube. When the HTCs inside and outside the tube reach  $20,000 \text{ W}/(\text{m}^2 \cdot \text{K})$  and  $5800 \text{ W}/(\text{m}^2 \cdot \text{K})$ , respectively, the TEM achieves its maximum output power of  $0.083 \text{ W}$  and efficiency of  $7.46\%$ . Therefore, enhancing the heat exchange performance of the fluids inside and outside the tube serves as a crucial factor in realizing the efficient utilization of LNG cold energy.

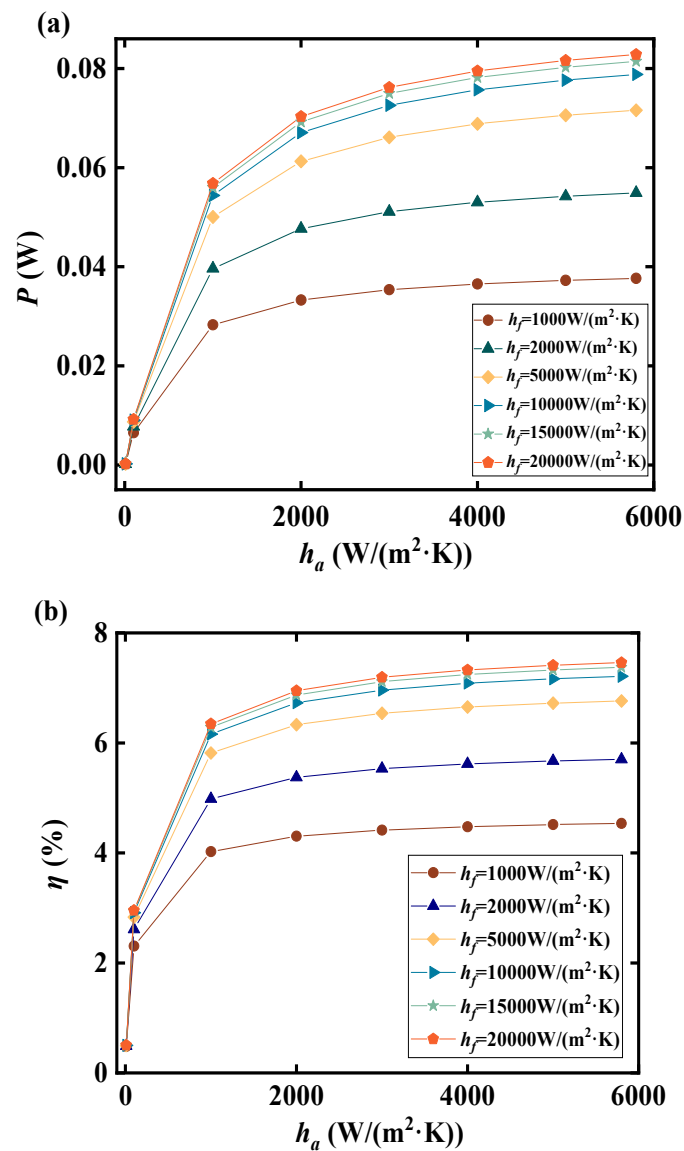


**Figure 10.** Variation of thermoelectric performance with HTC inside and outside the tube. (a) Output power. (b) Conversion efficiency.

The temperature variations corresponding to different HTCs inside and outside the tube are presented in Figure 11. Increasing the HTC outside the tube  $h_a$  effectively raises the temperature at the hot end of the TEL, thereby increasing the TDHC. Consequently, the HTC inside the tube  $h_f$  is increased to lower the temperature at the cold end of the TEL and further enhance the TDHC. However, it should be noted that, in relative terms, a higher HTC is required at the cold end due to the larger surface area of the hot end of the TEM. Overall, it is evident that when the HTCs inside and outside the tube reach  $h_f = 10,000 \text{ W/(m}^2\cdot\text{K)}$  and  $h_a = 4000 \text{ W/(m}^2\cdot\text{K)}$ , respectively, the conversion efficiency can reach 6.98%. Subsequent improvements in thermoelectric efficiency resulting from further escalation of the HTC are minimal. Additionally, it is important to consider that increased HTCs often necessitate additional energy consumption. Therefore, the design of thermoelectric generators for LNG cold energy recovery must consider the coupled effects of heat transfer, flow resistance, and thermoelectric conversion.

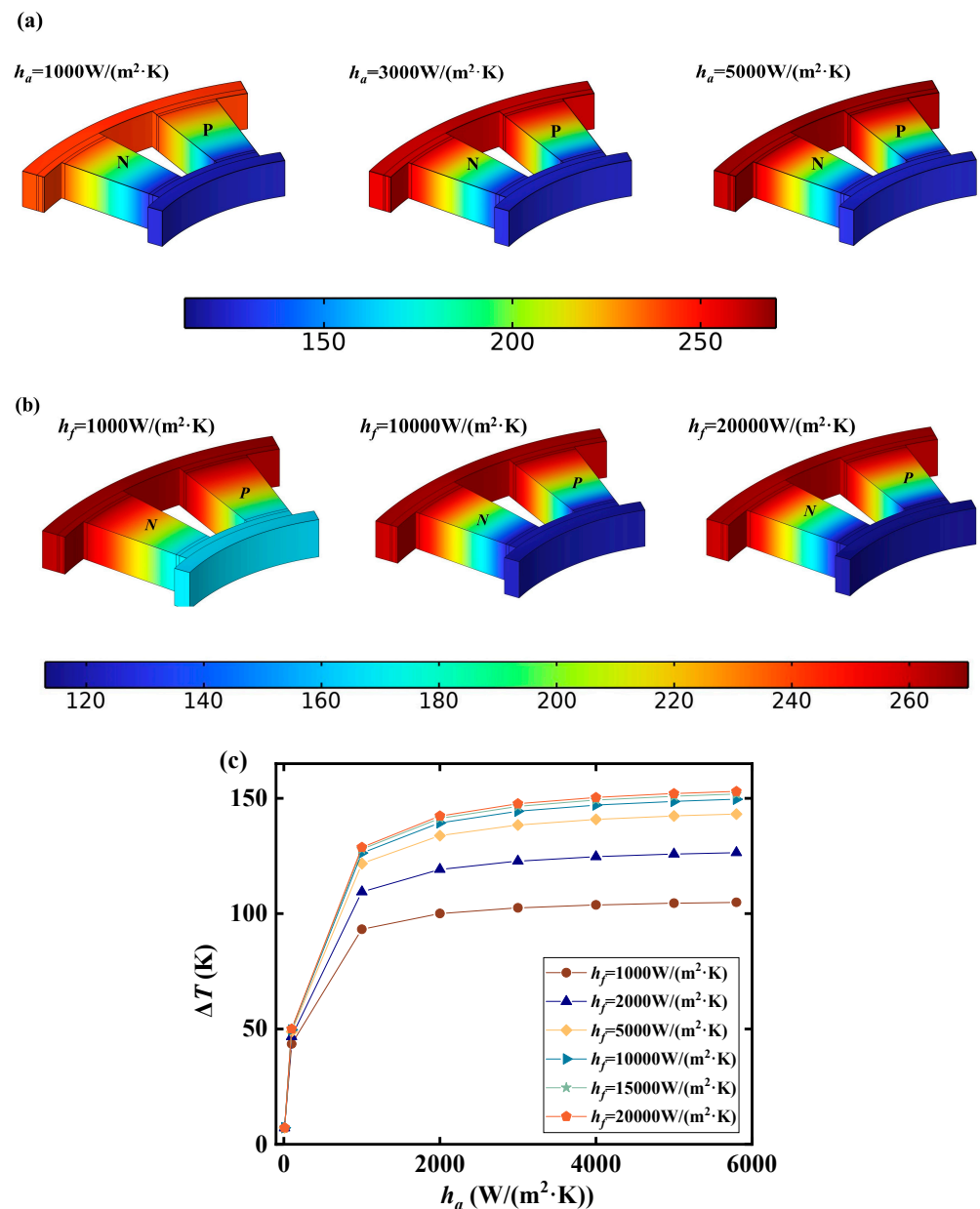


**Figure 11.** Variation of module temperature parameters with HTC inside and outside the tube. (a) Temperature cloud diagram outside the tube. (b) Temperature cloud diagram inside the tube. (c) Temperature difference between the hot and cold ends.

#### 4. Conclusions

The utilization of a gasifier coupled with a thermoelectric generator offers the opportunity to perform LNG gasification while concurrently generating electricity through cold energy recovery. The fundamental unit of the gasifier tube in this novel system is composed of an annular TEM. In this research, a mathematical model of the annular TEM is developed to investigate the influence of the TEMs structure and heat exchange conditions on its thermoelectric performance. The main findings are as follows:

1. The presence of an optimal load enables the optimization of the TEMs thermoelectric performance. The optimal load resistance increases as the height of the TEL increases. Additionally, the conversion efficiency demonstrates an increasing trend with higher TEL heights. However, there exists an optimal TEL height of 2 mm that maximizes the output power.

2. Increasing the central angle of the TEL leads to a rise in the TEMs output power but results in a decrease in conversion efficiency. Specifically, when the TEL central angle is increased from 8.5° to 14.5°, the TEMs output power experiences a 10.9% increase, while the conversion efficiency decreases by 22.34%.
3. The thermoelectric performance of the TEM can be significantly enhanced by improving the heat exchange of the fluid inside and outside the tube. When the HTC outside the tube reaches 4000 W/(m<sup>2</sup>·K) and the HTC inside the tube reaches 10,000 W/(m<sup>2</sup>·K), further increases in the HTCs yield minimal benefits. Therefore, when designing an innovative thermoelectric generator for LNG cold energy recovery, it is essential to consider the comprehensive performance aspects of heat transfer, flow resistance, and thermoelectric conversion.

**Author Contributions:** Y.Z.: Methodology, Writing—original draft. H.D.: Software, Data curation. W.L.: Software. Z.X.: Software. Q.Z.: Data curation. Y.W.: Writing—review and editing. M.G.: Conceptualization, Writing—review and editing. All authors have read and agreed to the published version of the manuscript.

**Funding:** This research was funded by the Natural Science Foundation of China (52206083), National Key Research and Development Program of China (2022YFE0119100), and Hebei Natural Science Foundation (E2021202143).

**Data Availability Statement:** The data presented in this study are available on request from the corresponding author.

**Acknowledgments:** The authors are grateful to the Natural Science Foundation of China (52206083), National Key Research and Development Program of China (2022YFE0119100), and Hebei Natural Science Foundation (E2021202143).

**Conflicts of Interest:** The authors declare no conflict of interest.

## References

1. Available online: <http://www.iea.org/> (accessed on 1 August 2023).
2. Gao, T.; Lin, W.; Gu, A. Improved processes of light hydrocarbon separation from LNG with its cryogenic energy utilized. *Energy Convers. Manag.* **2011**, *52*, 2401–2404. [[CrossRef](#)]
3. Pan, J.; Li, R.; Lv, T.; Wu, G.; Deng, Z. Thermal performance calculation and analysis of heat transfer tube in super open rack vaporizer. *Appl. Therm. Eng.* **2016**, *93*, 27–35. [[CrossRef](#)]
4. Liu, Z.; Karimi, I.A.; He, T. A novel inlet air cooling system based on liquefied natural gas cold energy utilization for improving power plant performance. *Energy Convers. Manag.* **2019**, *187*, 41–52. [[CrossRef](#)]
5. Wu, Y.; Xiang, Y.; Cai, L.; Liu, H.; Liang, Y. Optimization of a novel cryogenic air separation process based on cold energy recovery of LNG with exergoeconomic analysis. *J. Clean. Prod.* **2020**, *275*, 123027. [[CrossRef](#)]
6. Bian, J.; Yang, J.; Liu, Y.; Li, Y.; Cao, X. Analysis and efficiency enhancement for energy-saving re-liquefaction processes of boil-off gas without external refrigeration cycle on LNG carriers. *Energy* **2022**, *239*, 122082. [[CrossRef](#)]
7. Liu, Y.; Han, J.; You, H. Exergoeconomic analysis and multi-objective optimization of a CCHP system based on LNG cold energy utilization and flue gas waste heat recovery with CO<sub>2</sub> capture. *Energy* **2020**, *190*, 116201. [[CrossRef](#)]
8. Xie, C.; Zhang, L.; Liu, Y.; Lv, Q.; Ruan, G.; Hosseini, S.S. A direct contact type ice generator for seawater freezing desalination using LNG cold energy. *Desalination* **2018**, *435*, 293–300. [[CrossRef](#)]
9. Bao, J.; Yuan, T.; Zhang, L.; Zhang, N.; Zhang, X.; He, G. Comparative study of liquefied natural gas (LNG) cold energy power generation systems in series and parallel. *Energy Convers. Manag.* **2019**, *184*, 107–126. [[CrossRef](#)]
10. Lee, I.; Park, J.; You, F.; Moon, I. A novel cryogenic energy storage system with LNG direct expansion regasification: Design, energy optimization, and exergy analysis. *Energy* **2019**, *173*, 691–705. [[CrossRef](#)]
11. Lee, S.W.; Kwon, J.G.; Kim, M.H.; Jo, H. Cycle analysis and economic evaluation for seawater-LNG Organic Rankine Cycles. *Energy* **2021**, *13*, 121259. [[CrossRef](#)]
12. Ning, J.; Sun, Z.; Dong, Q.; Liu, X. Performance study of supplying cooling load and output power combined cycle using the cold energy of the small scale LNG. *Energy* **2019**, *172*, 36–44. [[CrossRef](#)]
13. Bao, J.; Lin, Y.; Zhang, R.; Zhang, N.; He, G. Strengthening power generation efficiency utilizing liquefied natural gas cold energy by a novel two-stage condensation Rankine cycle (TCRC) system. *Energy Convers. Manag.* **2017**, *143*, 312–325. [[CrossRef](#)]
14. Joy, J.; Kochunni, S.K.; Chowdhury, K. Size reduction and enhanced power generation in ORC by vaporizing LNG at high supercritical pressure irrespective of delivery pressure. *Energy* **2022**, *260*, 124922. [[CrossRef](#)]
15. Ma, G.; Lu, H.; Cui, G.; Huang, K. Multi-stage Rankine cycle (MSRC) model for LNG cold-energy power generation system. *Energy* **2018**, *165*, 673–688. [[CrossRef](#)]

16. Zhou, T.; Liu, J.; Ren, J.; Yang, S. Thermodynamic analysis and optimization of a multi-stage Rankine cycle power system combining with hydrate energy storage for liquefied natural gas cold energy utilization. *J. Energy Storage* **2022**, *56*, 105974. [[CrossRef](#)]
17. Choi, I.-H.; Lee, S.; Seo, Y.; Chang, D. Analysis and optimization of cascade Rankine cycle for liquefied natural gas cold energy recovery. *Energy* **2013**, *61*, 179–195. [[CrossRef](#)]
18. Qu, Z.; Bai, Y.; Pu, L. One-dimensional numerical study of thermal performance of an organic Rankine cycle system using liquefied natural gas as a cold source for cold energy recovery. *J. Nat. Gas Sci. Eng.* **2015**, *26*, 1399–1413. [[CrossRef](#)]
19. Yu, H.; Kim, D.; Gundersen, T. A study of working fluids for Organic Rankine Cycles (ORCs) operating across and below ambient temperature to utilize Liquefied Natural Gas (LNG) cold energy. *Energy* **2019**, *167*, 730–739. [[CrossRef](#)]
20. Zhao, Y.; Lu, M.; Li, Y.; Wang, Y.; Ge, M. Numerical investigation of an exhaust thermoelectric generator with a perforated plate. *Energy* **2023**, *263*, 125776. [[CrossRef](#)]
21. Luo, D.; Yan, Y.; Chen, W.-H.; Yang, X.; Chen, H.; Cao, B.; Zhao, Y. A comprehensive hybrid transient CFD-thermal resistance model for automobile thermoelectric generators. *Int. J. Heat Mass Transf.* **2023**, *211*, 124203. [[CrossRef](#)]
22. Kambe, M.; Morita, R.; Omoto, K.; Koji, Y.; Yoshida, T.; Noishiki, K. Thermoelectric Power Conversion System Combined with LNG Vaporizer. *J. Power Energy Syst.* **2008**, *2*, 1304–1319. [[CrossRef](#)]
23. Weng, C.-C.; Lin, M.-C.; Huang, M.-J. A waste cold recovery from the exhausted cryogenic nitrogen by using thermoelectric power generator. *Energy* **2016**, *103*, 385–396. [[CrossRef](#)]
24. Lin, M.-C.; Chen, H.-Y.; Chung, F.-T.; Huang, M.-J. A design and verification of a non-icing and non-condensing waste-cold-recovery system. *Appl. Therm. Eng.* **2021**, *197*, 117378. [[CrossRef](#)]
25. Lobunets, Y. Thermoelectric Generator for Utilizing Cold Energy of Cryogen Liquids. *J. Electron. Mater.* **2019**, *48*, 5491–5496. [[CrossRef](#)]
26. Chung, D.Y.; Hogan, T.; Brazis, P.; Rocci-Lane, M.; Kannewurf, C.; Bastea, M.; Uher, C.; Kanatzidis, M.G. CsBi<sub>4</sub>Te<sub>6</sub>: A high-performance thermoelectric material for low-temperature applications. *Science* **2000**, *287*, 1024–1027. [[CrossRef](#)]
27. Sun, W.; Hu, P.; Chen, Z.; Jia, L. Performance of cryogenic thermoelectric generators in LNG cold energy utilization. *Energy Convers. Manag.* **2005**, *46*, 789–796. [[CrossRef](#)]
28. Kambe, M.; Morita, R.; Omoto, K.; Koji, Y.; Yoshida, T.; Noishiki, K. Thermoelectric Module Performance in Cryogenic Temperature. *J. Power Energy Syst.* **2010**, *4*, 12–26. [[CrossRef](#)]
29. Karabetoglu, S.; Sisman, A.; Ozturk, Z.F.; Sahin, T. Characterization of a thermoelectric generator at low temperatures. *Energy Convers. Manag.* **2012**, *62*, 47–50. [[CrossRef](#)]
30. Jeong, E.S. Optimization of power generating thermoelectric modules utilizing LNG cold energy. *Cryogenics* **2017**, *88*, 29–35. [[CrossRef](#)]
31. Ge, M.; Wang, X.; Zhao, Y.; Wang, S.; Liu, L. Performance analysis of vaporizer tube with thermoelectric generator applied to cold energy recovery of liquefied natural gas. *Energy Convers. Manag.* **2019**, *200*, 112112. [[CrossRef](#)]
32. Chen, Z.; Li, M.; Guo, R.; Wang, Y.; Zhou, D.; Chen, Z.; Ang, R. Performance evolution of thermoelectric modules under constant heat flux. *Mater. Today Phys.* **2023**, *35*, 101136. [[CrossRef](#)]
33. Klimenko, V. A generalized correlation for two-phase forced flow heat transfer—Second assessment. *Int. J. Heat Mass Transf.* **1990**, *33*, 2073–2088. [[CrossRef](#)]
34. Gu, A. *Liquefied Natural Gas Technology Manual*; Machinery Industry Press: Beijing, China, 2004. (In Chinese)
35. Luo, T.; Wang, S.; Li, H.; Tang, X. Low temperature thermoelectric properties of melt spun Bi<sub>85</sub>Sb<sub>15</sub> alloys. *Intermetallics* **2013**, *32*, 96–102. [[CrossRef](#)]
36. Sidorenko, N.; Parashchuk, T.; Maksymuk, M.; Dashevsky, Z. Development of cryogenic cooler based on n-type Bi-Sb thermoelectric and HTSC. *Cryogenics* **2020**, *112*, 103197. [[CrossRef](#)]
37. Guo, S.; Li, H.; Lu, Y.; Liu, Z.; Hu, X. Lattice softening enables highly reversible sodium storage in anti-pulverization Bi-Sb alloy/carbon nanofibers. *Energy Storage Mater.* **2020**, *27*, 270–278. [[CrossRef](#)]
38. Jia, X.; Guo, Q. Design study of Bismuth-Telluride-based thermoelectric generators based on thermoelectric and mechanical performance. *Energy* **2019**, *190*, 116226. [[CrossRef](#)]
39. Xu, H.; Zhang, Q.; Yi, L.; Huang, S.; Yang, H.; Li, Y.; Guo, Z.; Hu, H.; Sun, P.; Tan, X.; et al. High performance of Bi<sub>2</sub>Te<sub>3</sub>-based thermoelectric generator owing to pressure in fabrication process. *Appl. Energy* **2022**, *326*, 119959. [[CrossRef](#)]

**Disclaimer/Publisher’s Note:** The statements, opinions and data contained in all publications are solely those of the individual author(s) and contributor(s) and not of MDPI and/or the editor(s). MDPI and/or the editor(s) disclaim responsibility for any injury to people or property resulting from any ideas, methods, instructions or products referred to in the content.